MODELING THE LOWER AND THE UPPER REGIME OF THE BLOOD UNIDIRECTIONAL FLOW IN MICRO-VESSELS

Gesse Arantes de Roure Neto

Francisco Ricardo da Cunha

gesse.roure@gmail.com

frcunha@unb.br

University of Brasilia - Department of Mechanical Engineering - Fluid Mechanics of Complex Flows Group - VORTEX - Microhydrodynamics and Rheology Lab

Campus Darcy Ribeiro, Distrito Federal, Brazil

Abstract. *There is a formation of a cell-depleted layer adjacent to micro-vessel walls during blood flow in regime of creeping flow. This biological layer is of vital importance in the transport of oxygen-saturated red cells to the unsaturated tissues. In this work, we first discuss the physical mechanisms in this creeping flow which lead to the formation of a cell-depleted layer. The main non-dimensional physical parameter governing the layer formation are presented from a simple model of predicting the layer thickness in steady state. In particular, we study the blood flow in two different scales (i.e. lower and upper bound limit) of the in vitro-microcirculation. For this end we examine the capillary core flow solution in which the inner fluid is considered a non-Newtonian one facing a small annular gap of a Newtonian plasma. This model is a good approximation for the blood flow occurring in the length scales of venules and arterioles diameters. In addition, we also propose a model for smaller vessels, like capillaries with diameter of few micrometers. In this lower bound limit we consider a periodic configuration of lined up paraboloidal cells moving in a flow under regime of lubrication approximation. So, the boundary condition in this lower flow limit considers the cell velocity and a numerical integration is used to solve the volumetric flux as a function of the pressure drop inside the capillary. The effect of the cell volume fraction in terms of the depleted layer thickness and cell aggregations is also investigated with this model. The influence of the wall irregularities on the flow is studied by using a simple sinusoidal model for the wall. Finally, an intrinsic viscosity of the blood is predicted theoretically for both the lower and upper bound regimes as a*

function of the non-dimensional vessel diameter, in good agreement with previous experimental works. We compare our theoretical predictions with experimental data and obtain a qualitative good for the classic Fahraeus-Lindqvist effect. A possible application of this work could be in illness diagnosis by evaluating of changes in the intrinsic viscosity due to blood abnormalities.

Keywords: *blood, hydrodynamic diffusion, non-Newtonian, rheology, cell-depleted layer*

1   Introduction

Blood can be defined as a suspension of cells in Newtonian plasma exhibiting a non-Newtonian behavior in which its rheological properties can be affected by several factors. Some diseases, such as diabetes, sickle cell anemia, malaria, and some kinds of cancer, directly alter blood rheological properties (Klingel et al., 2000). Thus, the rheology of blood constitutes an interesting object of study, since it allows relating changes in its flow behavior with certain pathologies. The study of microcirculation in particular is of extreme importance, as 80% of the pressure drop between the aorta and the vena cava happens within the microcirculation (Sung et al., 1982), where the most interesting rheological phenomena occurs (Popel and Johnson, 2005).

The blood cells are classified into 3 main types: erythrocytes, leukocytes and platelets. The erythrocytes, also known as red cells, are the responsible for the oxygen transportation throughout the body. Their scale is larger than the other blood cells, and they correspond to 40% to 45% of the total volume of blood in a healthy human being. The leukocytes, or white cells, function is to combat body infections. The platelets contribute to blood's coagulation and to seal disrupted areas inside the vessels.

The sum of leukocytes and platelets corresponds to less than 1% of the total blood volume. Therefore, the erythrocytes are the cells that are more relevant to determine the rheological properties of the blood (Skalak et al., 1989). The volume fraction occupied by the erythrocytes is called hematocrit.

The red cells in a non-deformation state, that is, in the absence of flow, exhibit a biconcave disc shape, with a diameter between 7 μm and 8 μm, and thickness of approximately 2.5 μm at the border and 1 μm at the center.

Blood flows in a network of multiple vessel scales. There are five different types of blood vessels in the human circulatory system: arteries, arterioles, veins, venules and capillaries. Veins and arteries hold the largest diameters, being related to the macrocirculation, while arterioles, venules and capillaries are related to the microcirculation. Venules and arterioles have an approximate diameter of 100 μm and capillary vessel diameter is at the same order of the erythrocytes length scale, even smaller than the red cells diameter.

Figure 1 shows real blood flowing through the vessels in microcirculation for different vessel sizes. It is clear the presence of a cell-depleted layer adjacent to the wall.

Due to the difference between scales within microcirculation, it is appropriate to consider two distinct approaches: a cell approach in the micro scales for the study of blood flow in capillaries, wherein red cells are assigned as isolated bodies in the Newtonian fluid; and a continuum approach to the study of venules and arterioles, where the blend of plasma and erythrocytes is considered as an equivalent continuum non-Newtonian fluid. Furthermore, it is relevant to consider the effect caused by a cell-depleted layer near the vessel walls. This region is formed due to the balance between two physical mechanisms: the hydrodynamic diffusion mechanism (Cunha and Hinch (1996), Acrivos et al. (1992)) and the migration of the particles away from the wall in the presence of a shear rate (Chan and Leal (1979), Smart and Leighton Jr (1991), Chaffey et al. (1965)). The existence of this region generates variations on the intrinsic fluid viscosity, creating the effect known as Fåhræus-Lindqvist Effect (Fåhræus and Lindqvist,
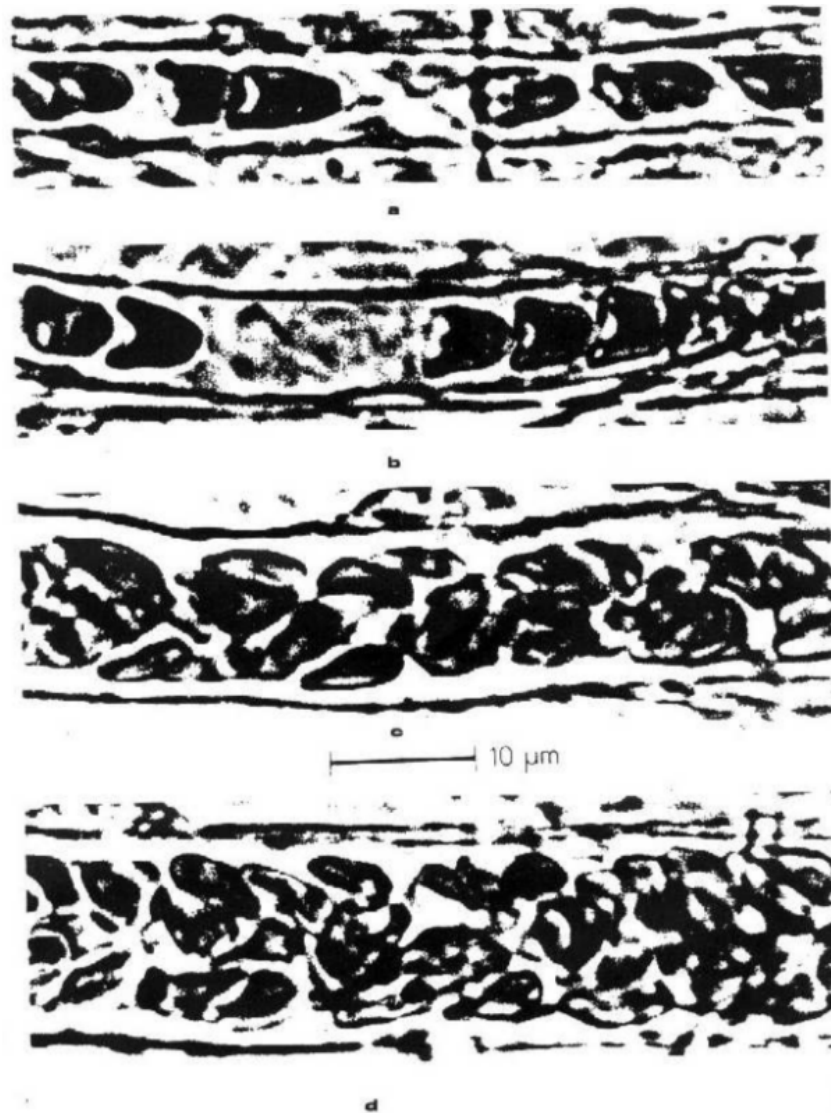
Figure 1: Micrography of blood flowing in different vessel sizes.

1931).

In this work, we present a discussion on the cell diffusion and migration mechanics in order to explain the origin of the formation of the layer free of cell adjacent to the vessel wall. We identify the important physical parameter for controlling the layer formation and a prediction of the steady state depleted layer thickness.

In addition, we use two different models for solving the flow for two asymptotic limit of the microcirculation mentioned above: the lower bound or cell scale and the upper bound or continuum scale. We predict the minimum value of the intrinsic viscosity by the matching between the two asymptotic limits and use our theoretical calculations to fit experimental data. A good agreement can be observed.

1.1   Dimensional Analysis

In this section, we show that the motion of the blood in regime of microcirculation is typically a creeping flow.

The physiological pressure gradient is approximately $\Delta p/l \approx 60$ mmHg/cm and a typical value for the vessel radius is $R = 100\ \mu$m. From Poiseuille's law it is possible to estimate a local shear rate given by $\dot{\gamma} = R\Delta p/(8\mu_p l) \approx 10^4$ s^{-1} as the plasma viscosity and density are approximately the same of the water. For a typical length of a red cell (a=5 μm) the particle Reynolds number $Re = \rho\dot{\gamma}a^2/\mu_p$, results in a value approximately 0.1, that corresponds to a creeping flow regime. Actually this conditions leads to a very short entrance length, keeping the flow unidirectional and free of inertial effects from the particles.

2 Formation of the Cell-Depleted Layer

Experimental observations show the existence of a cell-depleted layer near the vessel walls in microcirculation blood flow. This layer affects the pressure drop through the vessel significantly, which makes the blood appear to be less viscous then it really is. This effect can be described as a combination of two physical phenomena: one which scatters the cells througout the vessel, called hydrodynamic diffusion, and the other which repels them far from the walls, called particle migration or drift.

In order to examine the particle hydrodynamic migration-diffusion, we first derive the equivalent diffusion-convection equation. We also show the general theory for determining the particle hydrodynamic diffusivity (Cunha and Hinch, 1996) and particle drift velocity, respectively. In order to estimate the size of the cell-depleted layer in a simple shear flow bounded by a rigid plane wall , we use drops of high viscosity ratio as cell prototypes. Indeed real cells have a high viscosity ratio between the membrane viscosity and the newtonian plasma viscosity. At higher shear rates, the cells rotate much faster than they deform by the factor $1/\lambda$.

2.1 Governing Equation for the Transport Problem

We now discuss an equation for the macroscopic migration-diffusion problem. This equation can be used to predict the thickness of the cell or particle-depleted layer near a wall.

The well-known advection-diffusion equation is given in general form by:

$$\frac{\partial \phi}{\partial t} + \nabla \cdot (\boldsymbol{u}\phi) = -\nabla \cdot \boldsymbol{\mathfrak{F}} \tag{1}$$

Where ϕ is the particle volume fraction. In the present context, $\boldsymbol{u}$ is the migration velocity of the drops, which is a combination of the flow velocity with the drift velocity away from the drop. The constitutive equation for the flux $\boldsymbol{\mathfrak{F}}$ is given by the classical Fick's law, namely

$$\boldsymbol{\mathfrak{F}} = -\boldsymbol{D} \cdot \nabla\phi, \tag{2}$$

where $\boldsymbol{D}$ is a second-rank tensor called the diffusivity tensor. Hence, the equation takes the following form:

$$\frac{\partial \phi}{\partial t} + \nabla \cdot (\boldsymbol{u}\phi) = \nabla \cdot (\boldsymbol{D} \cdot \nabla \phi), \tag{3}$$

which is the general form of a sourceless advection-diffusion equation.

Hydrodynamic Diffusivity

The hydrodynamic diffusion phenomenon, in contrast with ordinary diffusion, has its origins not in the molecular scale, but in the microhydrodynamical scales (Davis, 1996). When two spherical particles interact with each other in creeping flow there is usually a kinematic reversibility. However, this symmetry can be broken. Some of the parameters that can break this symmetry are: particle deformation, roughness, non-spherical particles, three-body interactions. This symmetry breaking causes a displacement of the original particle trajectory. When many particles interact with each other, these particles start to random walk among the streamlines. This random walk is what causes the self-diffusion of the particles.
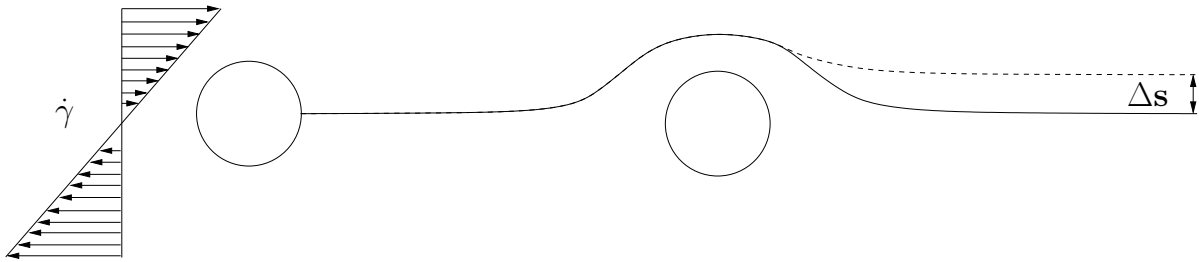
Figure 2: Displacement for the original trajectory due to symmetry breaking. The solid line represents the relative trajectory with kinematic reversibility. The dashed line represents the actual relative particle trajectory.

However, unlike ordinary diffusion, the self-diffusion does not coincide with $\boldsymbol{D}$. Acctually, $\boldsymbol{D}$ is given by 2 times the self diffusivity plus a down-gradient diffusivity contribution (Cunha and Hinch, 1996):

$$\boldsymbol{D} = 2\boldsymbol{D}^S + \boldsymbol{D}^{DG}, \tag{4}$$

given in the general form for a simple shear by the functional relation

$$\boldsymbol{D} = \phi\dot{\gamma}a^2 f[\boldsymbol{s}], \tag{5}$$

where $\boldsymbol{s}$ is the position of a tracked particle and the square brackets indicate a functional relation. In the problem of simple shear, the diffusivity tensor has two main directions and one null direction. The general expression to calculate theoretically the hydrodynamic diffusivity from the analysis of two interacting particle relative trajectories is given by (Cunha and Hinch, 1996):

$$\boldsymbol{D} = \frac{3}{4\pi} \int_{-\infty}^{\infty} \int_{-\infty}^{\infty} \left(\Delta\boldsymbol{s}\Delta\boldsymbol{s}|x_2| + |\Delta s_2|x_2^2\hat{\boldsymbol{e}}_2\hat{\boldsymbol{e}}_2 + |\Delta s_3|x_3^2\hat{\boldsymbol{e}}_3\hat{\boldsymbol{e}}_3 \right) dx_2 dx_3 \tag{6}$$

Determination of the Drift Velocity

When a particle is submitted to an external flow, it generates disturbances in the velocity, pressure and stress fields. If a particle is force and torque free, the lowest order disturbance on the fields is due to the stresslet. The disturbance in the velocity field by a single stresslet is given by

$$\boldsymbol{u} = -\frac{3}{8\pi\mu}\boldsymbol{S} : \frac{\boldsymbol{rrr}}{r^5}, \tag{7}$$

where $\boldsymbol{S}$ is the particle stresslet, which is the symmetric and traceless part of the hydrodynamic dipole, related to the particle stress exerted on the fluid. This particle stresslet is given by the symmetric part of the integral

$$\int_{\partial D} \left[\boldsymbol{x}\left(\hat{\boldsymbol{n}} \cdot \boldsymbol{\sigma}\right) - \mu(\boldsymbol{u}\hat{\boldsymbol{n}} + \hat{\boldsymbol{n}}\boldsymbol{u}) \right] dS, \tag{8}$$

where ∂D is the surface of the particle. This integral depends on the shape and size of the particles, local traction and flow velocity evaluated on the particle surface. This disturbance in the velocity field does not satisfy the no-slip boundary condition on the plane. To correct this we can introduce an image system at the other side of the wall (Kim and Karrila, 2013) in order to satisfy the boundary conditions. The general form of the drift velocity induced by the the image system on the particle in this case is

$$\boldsymbol{u}^* = (\boldsymbol{S} \cdot \hat{\boldsymbol{n}}) \cdot (\alpha_1 \boldsymbol{1} + \alpha_2 \hat{\boldsymbol{n}}\hat{\boldsymbol{n}}) \tag{9}$$

In the case of a rigid wall, the constants α_1 and α_2 are given by:

$$\alpha_1 = -\frac{1}{8\pi\mu}\frac{3}{4s^2}, \qquad \alpha_2 = -\frac{1}{8\pi\mu}\frac{3}{8s^2}, \tag{10}$$

where s is the distance between the particle and the wall. Projecting the drift velocity on the normal component, we have:

$$\hat{\boldsymbol{n}} \cdot \boldsymbol{u}^* = -\frac{9}{64\pi\mu s^2}(\hat{\boldsymbol{n}}\hat{\boldsymbol{n}} : \boldsymbol{S}). \tag{11}$$

Thus, the bulk drift velocity $\boldsymbol{u}$ for the problem is given by:

$$u_y = -\frac{9}{64\pi\mu y^2} \langle S_{yy} \rangle \,, \tag{12}$$

where y is the coordinate that represents the distance between any point in space and the wall. The brackets represent a statistical average of the particle in a volume V^*. In this case, V^* is a volume which contains a large number of particles but small enough to be considered a point. Considering a statistically homogeneous suspension, this statistical average over the particles is given by:

$$\langle \boldsymbol{S} \rangle = \frac{1}{N} \sum_{\alpha} \boldsymbol{S}_{\alpha} \tag{13}$$

The average normal particle stress contribution $\langle S_{yy} \rangle$ can be calculated analytically under condition of small deformation and dilute regimes. For moderate and large particle deformations, a boundary integral method is required for the calculation of stresslet integral (Kennedy et al., 1994).

2.2 General Expression for the Particle-Depleted Layer Thickness in a 1-D Diffusion Problem

Now we develop a generic model for the size of the particle-free layer adjacent to a boundary of a sheared suspension of non-Brownian particles in a low Reynolds number.

The particle drift velocity can be written in a general form as

$$u_y = \dot{\gamma} a g(y). \tag{14}$$

In addition, the most general expression for the shear-induced diffusion is:

$$D = \dot{\gamma} a^2 \phi f[\boldsymbol{s}] \tag{15}$$

Under these conditions, the drift-diffusion equation (3) for a one dimensional diffusion simplifies to

$$\frac{d}{dy} \left(\dot{\gamma} a g(y) \phi \right) = \frac{d}{dy} \left(\dot{\gamma} a^2 \phi f[\boldsymbol{s}] \frac{d\phi}{dy} \right). \tag{16}$$

In terms of the non-dimensional length $\tilde{y} = y/a$:

$$\frac{d}{d\tilde{y}} \left(g(\tilde{y}) \phi \right) = \frac{d}{d\tilde{y}} \left(\phi f[\boldsymbol{s}] \frac{d\phi}{d\tilde{y}} \right) \tag{17}$$

Now, by a direct integration, using the boundary condition $\phi(\tilde{y} \to \infty) = \phi_\infty$, we obtain:

$$\phi(\tilde{y}) = \phi_\infty - \int_{\tilde{y}}^{\infty} \frac{g(t)}{f[\boldsymbol{s}]} dt, \qquad \text{for } \tilde{y} \geq \tilde{\delta} \tag{18}$$

$$\phi(\tilde{y}) = 0, \qquad \text{for } \tilde{y} \leq \tilde{\delta} \tag{19}$$

where ϕ_∞ is the particle volume fraction in the bulk suspension far from the boudary. Therefore, a particle-free layer is predicted and $\tilde{\delta}$ can be found by the following expression

$$\phi_\infty = \int_{\tilde{\delta}}^{\infty} \frac{g(t)}{f[\boldsymbol{s}]} dt \tag{20}$$

2.3 Prediction of the Particle-Depleted Layer Thickness for a Sheared Emulsion Near a Wall

Now, we apply the general theory described in sections 2.1 and 2.2 for the case of a dilute emulsion of high viscosity drops under condition of small deformation. The idea is to explore the balance of the main physical mechanisms of migration and diffusion by considering drops as being prototypes of cells. So, we study the drop-free layer adjacent to the wall when the dilute emulsion is undergoing a simple shearing flow. Figure 3 gives a sketch of the flow problem analyzed here.
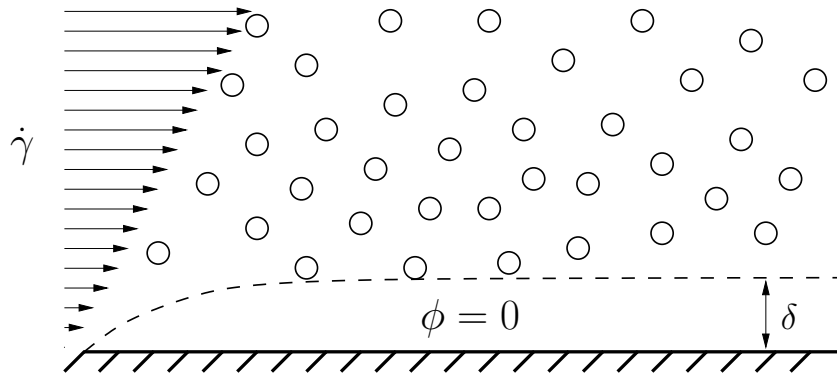
Figure 3: Formation of a particle-depleted layer near a wall in simple shear flow emulsion

Using the advection-diffusion equation, it is possible do predict the size of the particle-depleted layer near a plane wall. The governing equation (3) for the problem can be written in the following form:

$$\frac{\partial \phi}{\partial t} + \frac{\partial}{\partial x}\left(u_x \phi\right) + \frac{\partial}{\partial y}\left(u_y \phi\right) = \frac{\partial}{\partial y}\left(D \frac{\partial \phi}{\partial y}\right) \tag{21}$$

as in this problem there is only diffusion in the y direction. The diffusivity for this case is given by the expression

$$D = \phi \dot{\gamma} a^2 f(\lambda). \tag{22}$$

in which a is the radius of the drops and $f(\lambda)$ is a function of the viscosity ratio, being a specific case of the $f[s]$ in equation (15). For $f(\lambda)$ we use the relation proposed by Cunha & Hinch (Cunha and Hinch, 1996):

$$f(\lambda) = \lambda^{c_1} \left(c_2 + c_3 \log(\lambda) \right)^{c_4} \tag{23}$$

where c_1, c_2, c_3 and c_4 are constants given by:

$$c_1 = -0.2915$$
$$c_2 = 1.347$$
$$c_3 = 2/3$$
$$c_4 = -0.7012$$

For high viscosity ratio drops it is possible to calculate the drift velocity u_y using equation (12). The stresslet average $\langle \boldsymbol{S} \rangle$ is related with the particle stress tensor in the following form (Kim and Karrila, 2013):

$$\langle \boldsymbol{S} \rangle = \frac{1}{n} \boldsymbol{\sigma^p} \tag{24}$$

in which n is the number density of particles. For a dilute emulsion of high viscosity ratio, the 22 component of the particle stress tensor is given by (Schowalter et al., 1968):

$$\sigma_{22}^p = -\frac{16}{3} Ca \, \dot{\gamma} \mu \phi \, h(\lambda) \tag{25}$$

where:

$$h(\lambda) = \frac{9}{2240} \frac{(19\lambda + 16)(9\lambda^2 + 17\lambda + 9)}{(\lambda + 1)^3} \tag{26}$$

Hence, for the case of high viscosity ratio drops, using equations (12), (24), (25) and (26) the drift velocity is given by:

$$u_y = \frac{Ca \dot{\gamma} a^3}{y^2} h(\lambda), \tag{27}$$

It can be noticed that the drift velocity u_y can be written in terms of Taylor deformation $D_T = \frac{(19\lambda + 16)}{16(\lambda + 1)} Ca$ as

$$u_y = \frac{\dot{\gamma} a^3}{y^2} \frac{9}{140} (9\lambda^2 + 17\lambda + 9) D_T. \tag{28}$$

Actually, this shows explicitly a relation between drift velocity and particle deformation.

For the nondimensionalization of equation (21), the scales are chosen such as:

$$t \sim \frac{\mu a}{\sigma} \qquad \boldsymbol{x} \sim a \qquad \phi \sim \phi_\infty, \tag{29}$$

where σ is the surface tension of the drop and ϕ_∞ is the particle volume fraction far from the wall. Using the expressions (22) and (27) for the diffusivity and drift velocity, the nondimensional equation is given by:

$$\frac{\partial \tilde{\phi}}{\partial \tilde{t}} + Ca \frac{\partial}{\partial \tilde{x}} \left(\tilde{y} \tilde{\phi} \right) + Ca^2 h(\lambda) \frac{\partial}{\partial \tilde{y}} \left(\frac{\tilde{\phi}}{\tilde{y}^2} \right) = \frac{f(\lambda) \phi_\infty}{Pe} \frac{\partial}{\partial y} \left(\tilde{\phi} \frac{\partial \tilde{\phi}}{\partial \tilde{y}} \right). \tag{30}$$

Here, $Ca = \mu \dot{\gamma} a / \sigma$ is the capillary number and $Pe = \sigma a / (\mu D_0)$ is a hydrodynamic Peclet number (related to hydrodynamic diffusion). It can be noticed that in the case of shear induced diffusion where $D_0 = \dot{\gamma} a^2$ we have $Pe = Ca^{-1}$. This is related to the fact that the diffusion and the drift happen in the same scale of the flow. The same parameters that characterize the diffusion (λ and Ca) are the same that characterize the drift velocity. Considering the problem near the wall ($\tilde{y} \ll 1/\tilde{y}^2$) in steady state, equation (30) takes the form of a specific case of equation (17), written as:

$$Ca\, h(\lambda) \frac{\partial}{\partial \tilde{y}} \left(\frac{\tilde{\phi}}{\tilde{y}^2} \right) = f(\lambda) \phi_\infty \frac{\partial}{\partial y} \left(\tilde{\phi} \frac{\partial \tilde{\phi}}{\partial \tilde{y}} \right), \tag{31}$$

where $f[\boldsymbol{s}] = f(\lambda)$ and $g(y) = y^{-2} h(\lambda)$. By the general solution given by equation (18), we find:

$$\tilde{\phi} = \frac{Ca\, h(\lambda)}{\phi_\infty f(\lambda)} \left(-\frac{1}{\tilde{y}} + \frac{1}{\tilde{\delta}} \right) \qquad \text{for } \tilde{y} > \tilde{\delta}. \tag{32}$$

Therefore, we obtain an expression for the nondimensional thickness $\tilde{\delta}$ of the particle-depleted layer, given by:

$$\tilde{\delta} = \frac{Ca}{\phi_\infty} \frac{h(\lambda)}{f(\lambda)} \tag{33}$$

Equation (33) indicates that the important physical parameters identified by our simple model of drop-like-cell are the viscosity ratio and the capillary number. In this flow λ measures

the relative importance between time scales for rotation and deformation. For high viscosity suspension the particles rotates much faster than deforms and they do not breakup under shear flow (Oliveira and Cunha, 2011). Actually, the drop-like-cell rotates with the vorticity of the imposed shear with just a small amount of deformation. This small deformation is already sufficient to break the time reversibility of the particle relative trajectories producing a hydro-dynamic diffusion, and also to produce the amount of asymmetry of the particle stress close to wall which results in a particle drift. So, both mechanisms of particle migration have origin in the hydrodynamic scale (it is not molecular nature) and both depend on particle deformation, and consequently on the capillary number. These two fluxes (diffusional and drift) are in bal-ance near to the wall and it defines the thickness of the depleted layer as shown by equation (33). From equation (33) we can also argue that increasing the λ the δ tends to the decrease by the fact that higher viscosity ratios inhibit particle deformation. Deformation here is the essential mechanism to produce both diffusion and drift.

Figure 4 shows the concentration profile $\tilde{\phi}$ as a function of $\tilde{y}$ in the solution domain of the flow. The presence of the depleted layer close to the wall can be seen as $(y \to 0)$ as well as the linear increase of its thickness with Ca. The results also show the presence of a concentration gradient for $\tilde{y} \sim 1$ characterizing a boundary layer of particle concentration due to the balance between a diffusional flux and a particle migration, both mechanisms occurring on the hydrodynamic time scale and induced by particle deformation. Defining a parameter $\tilde{y}^*$ as being the value of $\tilde{y}$ corresponding to $\phi = 0.99\phi_\infty$ we define the thickness of the particle concentration boundary layer $\tilde{\delta}^* = \tilde{y}^* - \tilde{\delta}$. Again this parameter increases significantly as the Ca increases. From capillary varying form 0.4 to 0.6, δ^* has a increase of 50%

The upper bound limit of this concentration boundary layer is just the hematocrit of the bulk blood which was an imposed boundary condition.

3 Continuum Model

In this section, we examine the continuum modeling of pressure-driven blood flow in the regime of microcirculation, which corresponds to length scales of microvessels up to $100 \ \mu$m. Therefore, the model is an approximation to the blood flow in venules and arterioles, in which we model the core flow as a continuum non-Newtonian fluid and the cell-depleted layer as a Newtonian (i.e. pure plasma region) gap on the near wall region. In this model we assume that the depleted layer thickness is a given parameter of the flow geometry.

For the core flow, a standard generalized Newtonian fluid model proposed by Casson is used (Bird et al., 1977). In this model the yields stress effect due to cell-aggregate formation is mainly captured at low shear rates. In the regimes of moderate shear rates a shear thinning behavior of the blood dominates the yield stress. On the other hand, at high shear rate the model describe the blood as a bulk fluid with a constant viscosity depending on the hematocrit only (no shear rate dependence).

Fig 5 shows a sketch of the studied flow in regime of microcirculation. The main parameters and geometric quantities of the problem are: plasma viscosity μ_p, blood's bulk viscosity μ_0, cross section radius $R(z)$, average cross section radius R_0, core flow radius R_δ, cell-depleted layer thickness δ, Casson's radius R_B and the yield stress τ_0. The vessel walls are modeled
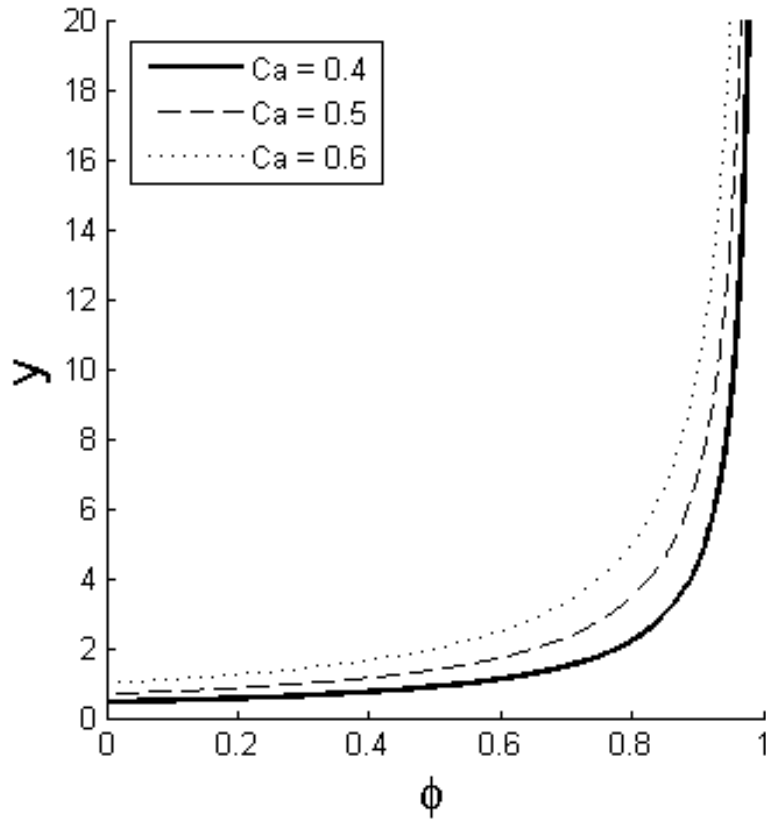
Figure 4: Steady-state particle concentration profile near a plane wall located in $\tilde{y} = 0$

considering a typical sinusoidal disturbance on the regular cylindrical geometry. So, under this condition the radius of the vessel is described by

$$R = R_0(1 + \alpha \sin(2\pi z/l)). \tag{34}$$

Now, the Cauchy's governing equation for an unidirectional flow in axisymmetric cylindrical coordinates is given by:

$$\frac{1}{r}\frac{\partial}{\partial r}(r\tau) = \frac{dp}{dz} = -G(z) \tag{35}$$

The viscous stress in eq. (35) is described by the following constitutive equation:

$$\tau = \eta(\dot{\gamma})\frac{\partial u}{\partial r} \tag{36}$$

where $\dot{\gamma} = (2\boldsymbol{E} : \boldsymbol{E})^{1/2}$ with $\boldsymbol{E}$ being the rate of strain tensor, i.e $\boldsymbol{E} = (\nabla\boldsymbol{u} + (\nabla\boldsymbol{u})^T)/2$, and the apparent viscosity η given by the Casson's model (Bird et al., 1977):
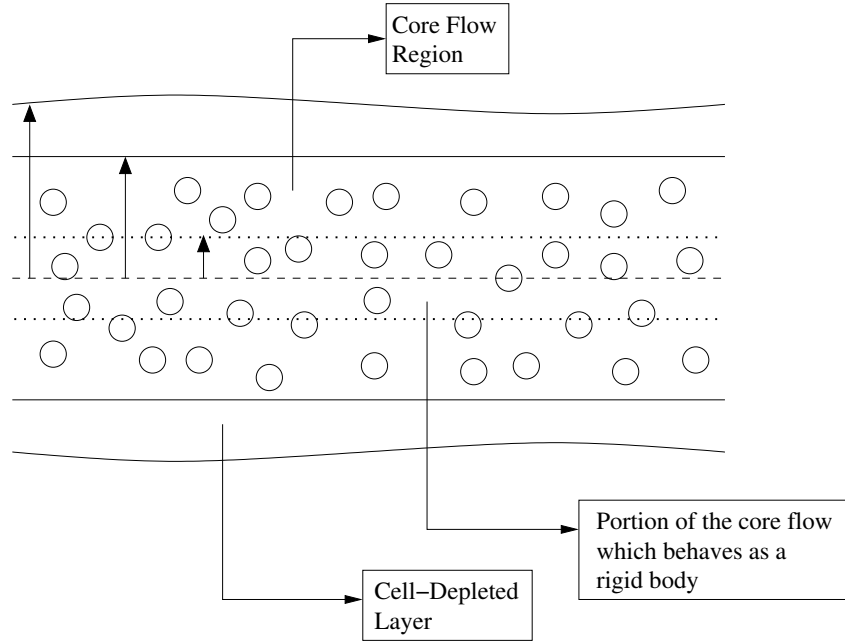
Figure 5: A sketch of the blood flow in a mcrovessel . The core flow of blood is modeled as a continuum non-Newtoinian fluid , whereas the cell-free layer of pure plasma adjacent to the wall is considered a typical Newtonian fluid.

$$\eta(\dot{\gamma}) = \begin{cases} \infty & \text{for } |\tau| \leq \tau_0 \\ \mu_\infty + \tau_0\dot{\gamma}^{-1} + 2\sqrt{\mu_\infty\tau_0}\dot{\gamma}^{-1/2} & \text{for } |\tau| > \tau_0. \end{cases} \tag{37}$$

The infinite viscosity for low shear stress represents an equilibrium condition due to the yields stress effect, in which the fluid only starts to flow when the shear stress modulus is above a certain value τ_0. Consequently, in the case of pressure driven flow in a micro-vessel, this creates a region $r < R_B$ in the cross section so that the fluid behaves like a rigid body. Solving equation (35) in terms of shear rate $\dot{\gamma}$ and applying the boundary condition of velocity and tangential viscous stress continuity, one finds:

$$\dot{\gamma}(r,z) = \begin{cases} 0 & \text{for } r \leq R_B \\ \dfrac{Gr}{2\mu_\infty} + \dfrac{GR_B}{2\mu_\infty} - \dfrac{GR_B^{1/2}}{\mu_\infty}r^{1/2} & \text{for } R_B < r \leq R_\delta \\ \dfrac{Gr}{2\mu_p} & \text{for } R_\delta < r \leq R \end{cases} \tag{38}$$

Now, the volumetric rate of the flow can be calculated by:

$$Q = \pi \int_0^R r^2\dot{\gamma}dr. \tag{39}$$

Solving the integral (39) for the solution presented in (38) we found:

CILAMCE 2016

Proceedings of the *XXXVII Iberian Latin-American Congress on Computational Methods in Engineering*
Suzana Moreira Ávila (Editor), ABMEC, Braslia, DF, Brazil, November 6-9, 2016

$$Q = \frac{\pi G R_\delta^4}{8\mu_\infty} \mathcal{A}\left(\frac{R_B}{R_\delta}\right) + \frac{\pi G}{8\mu_p}\left(R^4 - R_\delta^4\right). \tag{40}$$

Here, $\mathcal{A}(x)$ is a function given by:

$$\mathcal{A}(x) = 1 + \frac{4}{3}x - \frac{17}{7}x^{1/2} - \frac{1}{21}x^4. \tag{41}$$

In order to write the solution in terms of non-dimensional quantities we shall use as the reference a standard Poiseuille flow of water in a tube of radius R_0. So, let's consider the following non-dimensional quantities by using the references values, R_0 and μ_w:

$$\tilde{G} \equiv \frac{G}{\dfrac{8Q\mu_w}{\pi R_0^4}} \; ; \; \tilde{R} \equiv \frac{R}{R_0} \; ; \; \tilde{\mu} \equiv \frac{\mu}{\mu_w}$$

Nondimensionalization of equation (40) leads to

$$\tilde{R}^4 = \tilde{\mu}_p \frac{1}{\tilde{G}} - \frac{\chi^4 \tilde{\mu}_p}{\tilde{\mu}_\infty}\mathcal{A}\left(\frac{\Omega Re_w}{\chi \tilde{G}}\right) + \chi^4, \tag{42}$$

which is a non-linear equation for the nondimensional pressure gradient $\tilde{G}$. The non-dimensional parameters appearing in eq (42) are:

$$\chi \equiv \frac{R_\delta}{R_0} \; ; \; Re_w \equiv \frac{\rho \bar{U} R_0}{\mu_w} \; ; \; \Omega \equiv \frac{\tau_0}{4\rho_w \bar{U}^2} \; ,$$

where ρ_w is the density of the water and $\bar{U} \equiv Q/\pi R_0^2$ is the mean velocity of the flow. The parameter χ is related with the size of the region occupied by the bulk blood, Re_w is the Reynolds number based of the vessel radius and the water viscosity. Ω is the parameter that controls the yield stress.

3.1 Computation of the Intrinsic Viscosity

It is well-know that for an incompressible Newtonian fluid flowing through a cylindrical capillary tube of radius R with a constant volumetric flow rate, the pressure drop is linear with the fluid viscosity for a given length ℓ. This relation is given by the classic Poiseuille's law, namely:

$$\mu = \frac{\pi R^4}{8Q\ell}\Delta p. \tag{43}$$

In the case of the problem in study, neither the vessel radius is constant nor the viscosity. However, Poiseuille's law can be used for defining an intrinsic viscosity term as being:

$$\mu_i \equiv \frac{\pi R_0^4}{8Q\ell}\Delta p = \frac{\pi R_0^4}{8Ql}\int_0^\ell Gdz \tag{44}$$

Defining the aspect ratio $\tilde{z} = z/\ell$, one finds:

$$\tilde{\mu}_i = \int_0^1 \tilde{G}(\tilde{z})d\tilde{z}. \tag{45}$$

Here, $\tilde{\mu}_i$ is nondimensionalized by the viscosity of the water. Note that the calculation of a non-dimensional intrinsic viscosity requires only the integration of the non-dimensional pressure gradient along the aspect ratio $\tilde{z}$.

It is instructive to note that (42) is a transcendental equation to be solved in terms of $\tilde{G}$. So $\tilde{G}$ is straightforward to be calculated analytically. However, in the limit case of $\Omega = 0$ and $\alpha = 0$ (i.r. $\tilde{R} = 1$) the intrinsic viscosity reduces simply to:

$$\tilde{\mu}_i = \frac{\tilde{\mu}_p}{1 + \chi^4 \left[\dfrac{\tilde{\mu}_p}{\tilde{\mu}_\infty} - 1\right]}. \tag{46}$$

Considering that the result given by equation (46) is only valid on the larger scales of microcirculation, where $\delta/R_0 \ll 1$, the geometric parameter χ^4 can be assymptoticaly expanded by the use of a binomial series $O(\delta/R_0)^2$ as follows:

$$\chi^4 = \left(1 - \frac{\delta}{R_0}\right)^4 \approx 1 - 4\frac{\delta}{R_0} \tag{47}$$

Consequently, the asymptotic expression for μ_i from (46) results in:

$$\tilde{\mu}_i = \frac{\tilde{\mu}_\infty}{1 + 4\dfrac{\delta}{R_0}\left[\dfrac{\tilde{\mu}_\infty}{\tilde{\mu}_p} - 1\right]} \tag{48}$$

This expression was calculated previously by several authors (Popel and Johnson, 2005). However, we have shown that in a more general condition of the blood flow in microcirculation, the intrinsic viscosity should be calculated by the numerical integration of equation (44).

4   Cell Approach

In this section we examine a model of blood flow from the cell scale approach. In this regime the vessel diameter is of the same order of the cell size. In this case, the cells usually

have to bend before enter the vessel. Figure 1 illustrates this regime of flow in the microcirculation also studied previously by Secomb and co-authors (Pries et al., 1994). The lined up cells configuration in the flow is approximately axisymmetric.

Based on experimental observation shown in figure 1 we propose a theoretical model to study the blood flow on these scales. The assumption of this model is that the blood flow consists of lined up rigid cells moving on Newtonian plasma in a periodic configuration with period $l + s$. Although the cells are not rigid, we assume that the reach a steady state of deformation as they enter into the vessel. Figure 6 presented a sketch of the flow problem that we studied in the lower regime of the microcirculation.
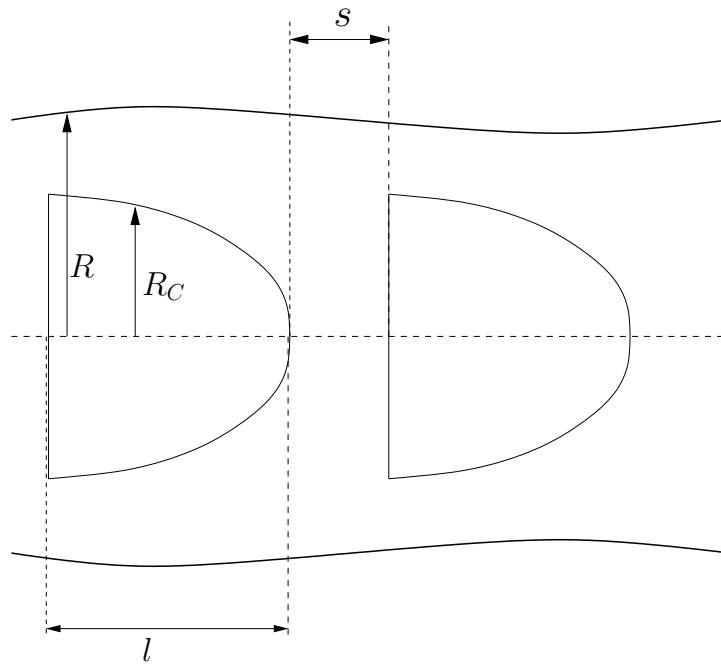
Figure 6: Lined up cells model for the blood flow in capillaries.

Even with those assumptions, the problem is still hard to be solved analytically due to the complex geometry of the flow domain. In addition, we assume that the lubrication approximation can be applied for the motion of the fluid in the gap between cell-wall. This is justified by the dimensional analysis of the flow, since the lubrification approximation only requires that $Re(a/L) \ll 1$. As the particle Reynolds number is 0.1 and $a/\ell \ll 1$, this hypothesis is valid.

The governing equation for the flow under regime of lubrication is given by:

$$\mu_p \nabla^2 \boldsymbol{u} = \nabla p, \tag{49}$$

subject to the no-slip and impenetrability boundary conditions at the surface of the cells and the vessel walls. Under condition of lubrication approximation and for a flow free of inertia at the full domain, we can split the problem in two parts:

$$
\begin{cases}
\mu_p \dfrac{1}{r} \dfrac{\partial}{\partial r}\left(r\dfrac{\partial u}{\partial r}\right) = \dfrac{\partial p}{\partial z} \equiv -G(z) & \\
u(R_C(z), z) = U_C & \text{(b.c. on the cell surface)} \\
u(R(z), z) = 0 & \text{(b.c. on the vessel wall)}
\end{cases}
\tag{50}
$$

in the gap between the cell and the vessel wall and

$$
\begin{cases}
\mu_p \dfrac{1}{r} \dfrac{\partial}{\partial r}\left(r\dfrac{\partial u}{\partial r}\right) = \dfrac{\partial p}{\partial z} \equiv -G(z) & \\
u(R(z), z) = 0 & \text{(b.c. on the vessel wall)}
\end{cases}
\tag{51}
$$

in the region between two cells. Equations (50) and (51) are connected to each other by the continuity equation, which in incompressible media requires that the volumetric flow rate must be equal in all transverse sections of the vessel.

These differential equations subjected to these boundary conditions are called pseudo partial differential equations, as they are just ordinary differential equations, as a direct consequence of the independence of u on z and p on r due to the unidirectional character of a flow free of inertia. Therefore the general solution for the velocity field inside the vessel is given by :

$$
u = -\frac{Gr^2}{4\mu_p} + C_1 \log(r) + C_2
\tag{52}
$$

As the interest is to calculate the volumetric flow rate, it is not necessary to know the value of C_2, due to (40). In the region of the gap, C_1 vanishes as a direct consequence of the continuity of the velocity. On the other hand, in the region of the gap between the cell and the vessel wall, we have

$$
C_1 = \frac{G}{4\mu_p \log(R/R_C)}(R^2 - R_C^2) - \frac{U_C}{\log(R/R_C)}
\tag{53}
$$

Using (40), it is straightforward to find that the volumetric flow rate is given by

$$
Q = \frac{\pi G R^4}{8\mu_p}
\tag{54}
$$

in the gap region and

$$
Q = \frac{\pi G}{8\mu_p}\mathcal{B}(z) + \pi U_C \mathcal{C}(z)
\tag{55}
$$

in the cell region, where

$$\mathcal{B}(z) = R^4 - R_C^4 - \frac{(R^2 - R_C^2)^2}{\log(R/R_C)} \tag{56}$$

and

$$\mathcal{C}(z) = \frac{R^2 - R_C^2}{2\log(R/R_C)} \tag{57}$$

The nondimensionalization of the volumetric flow rate is made in the same way as described in section 3. The same scale are used here, except the one of z. Here, the appropriate longitundinal length scale is the l of the cell. By doing this, the non-dimensional pressure gradient is represented in the following form

$$\tilde{G}_s = \frac{\tilde{\mu}_p}{\tilde{R}^4} \tag{58}$$

in the region of the gap and

$$\tilde{G}_l = \tilde{\mu}_p \left(\frac{1 - \bar{U}_C \tilde{\mathcal{C}}(\tilde{z})}{\tilde{\mathcal{B}}(\tilde{z})} \right) \tag{59}$$

in the cell region. Using the definition for intrinsic viscosity in (44), one finds:

$$\tilde{\mu}_i = \frac{1}{1 + \tilde{s}} \left[\int_0^1 \tilde{G}_l d\tilde{z} + \int_1^{1+\tilde{s}} \tilde{G}_s(\tilde{z}) d\tilde{z} \right] . \tag{60}$$

Depending on the cell profile, the integral of G_l is not straightforward to be calculated analytically, so it is convenient use a numerical integration method in order to compute the intrinsic viscosity. In the result section we shall present numerical results of the intrinsic viscosity as a function of the vessel/cell aspect ratio. The solutions are obtained by numerical integration based on a simple trapezoidal rule.

4.1 Cell Aggregation

Our lined cells model can be used to predict the effects of cell aggregation on the intrinsic viscosity. Considering the flow as having a periodic domain, the volume fraction is given by the ratio between the volume of the cell and the volume of the lattice. In terms of nondimensional quantities, we have:

$$\phi = \frac{\displaystyle\int_0^1 \tilde{R}_C^2 d\tilde{z}}{\displaystyle\int_0^{1+\tilde{s}} \tilde{R}^2 d\tilde{z}} \tag{61}$$

It should be important to note that the hematocrit ϕ depends on the geometric parameter $\tilde{s}$. For a cylindrical cell of constant $\tilde{R}_C$ and a cylindrical vessel of constant $\tilde{R} = 1$, we have:

$$\phi = \frac{\tilde{R}_C^2}{1+\tilde{s}} \tag{62}$$

Under this condition, the intrinsic viscosity reduces to:

$$\tilde{\mu}_i = \tilde{\mu}_p + \left(\tilde{G}_l - \tilde{\mu}_p\right)\frac{\phi}{\tilde{R}_C^2} \tag{63}$$

So, for the case of a constant radius vessel and a cylindrical cell, the relation between the intrinsic viscosity and the cell volume fraction is linear. The expression (63) is similar to an effective viscosity $O(\phi)$ as predicted by Einstein (Einstein, 1956) for a dilute statistically homogeneous suspension undergoing linear shear. Since we have considered the motion of undeformed cells in the absence of hydrodynamic interaction between them, an $O(\phi)$ correction due to the presence of the cell must persist for any steady state geometry of our model. It is interesting, however, that our coefficient $(\tilde{G}_l - \tilde{\mu}_p)/\tilde{R}_C^2$ depends on the flow properties and geometry. So, this coefficient is not universal and clearly a non-local quantity, even for the case of non-interacting cells. In the present context, the general calculation $O(\phi)$ of the intrinsic viscosity for an arbitrary permanent cell profile moving in a microvessel of constant radius is found to be

$$\tilde{\mu}_i = \tilde{\mu}_p + \left(\int_0^1 \tilde{G}_l d\tilde{z} - \tilde{\mu}_p\right)\frac{\phi}{\displaystyle\int_0^1 \tilde{R}_C^2 d\tilde{z}}. \tag{64}$$

It has to be noticed that the model only predicts values of ϕ between the range from 0 to $\int_0^1 \tilde{R}_C^2 d\tilde{z}$. In general, for periodic configurations, $\tilde{\mu}_i$ is linear with respect to ϕ. Considering the vessel with a periodic disturbance to account the effect of the vessel roughness, the most general way to write the intrinsic viscosity is in the form:

$$\tilde{\mu}_i = \tilde{\mu}_p\left[A(\alpha) + \phi B(\alpha)\right] \tag{65}$$

with

CILAMCE 2016

Proceedings of the *XXXVII Iberian Latin-American Congress on Computational Methods in Engineering*
Suzana Moreira Ávila (Editor), ABMEC, Braslia, DF, Brazil, November 6-9, 2016

$$A(\alpha) = \frac{1}{1+\tilde{s}} \int_0^{1+\tilde{s}} \tilde{R}^{-4} d\tilde{z} \tag{66}$$

and

$$B(\alpha) = \frac{1}{1+\tilde{s}} \frac{\int_0^{1+\tilde{s}} \tilde{R}^2 d\tilde{z}}{\int_0^1 \tilde{R}_C^2 d\tilde{z}} \int_0^1 \left[\frac{1 - \tilde{U}_C \tilde{\mathcal{C}}(\tilde{z})}{\tilde{\mathcal{B}}(\tilde{z})} - \tilde{R}^{-4} \right] d\tilde{z}. \tag{67}$$

Owing to the fact that $\tilde{R}$ is a function of $\tilde{z}/(1+\tilde{s})$, it is straightforward to show by a simple change of coordinates that A and B are only functions of the variable α, any other dependence with the geometry is purely functional. In the case of a non disturbed vessel, the intrinsic viscosity has the form $\mu_i = \mu_p (1 + B_0 \phi)$, with

$$B_0 = \left[\int_0^1 \tilde{R}_C^2 d\tilde{z} \right]^{-1} \int_0^1 \left[\frac{1 - \tilde{U}_C \tilde{\mathcal{C}}(\tilde{z})}{\tilde{\mathcal{B}}(\tilde{z})} - 1 \right] d\tilde{z}. \tag{68}$$

In general, the vessel profile can be written in the following form:

$$\tilde{R} = 1 + \alpha f \left(\frac{\tilde{z}}{1+\tilde{s}} \right) \tag{69}$$

where $\alpha \ll 1$ and $f(x)$ a periodic function in $x \in [0,1]$ and amplitude $O(1)$, with

$$\int_0^1 f(x) dx = 0 \tag{70}$$

In this paper, we consider the simple case of a single harmonic mode disturbance with $f(x) = \sin(2\pi x)$, but this holds in general, as any periodic disturbance can be represented accurately by a Fourier series.

5 Numerical Results

In this section, we examine results for the two previously presented models. First comparing the numerical results for the models with experimental data, then using the models to predict variations in the intrinsic viscosity due to the change of roughness, yield stress and plasma viscosity.

5.1 Fåhræus - Lindqvist effect

The Fåhræus-Lindqvist effect (Fåhræus and Lindqvist, 1931) predicts a change of viscosity due to a variation in the vessel radius. With the two models presented on this paper, it is possible to predict such changes in the smaller and larger scales of the microcirculation.

Figure 7 shows the results for the two models with constant cross section radius $R = R_0$ in the absence of yield stress. These results are compared with results from the experiments carried out by Pries (Pries et al., 1994) on in-vitro blood flow. We consider a value of $\delta = 1 \ \mu$m and $R_C = 1.25 \ \delta$ in order to fit the results. With R_C being the maximum value of $R_C(z)$.
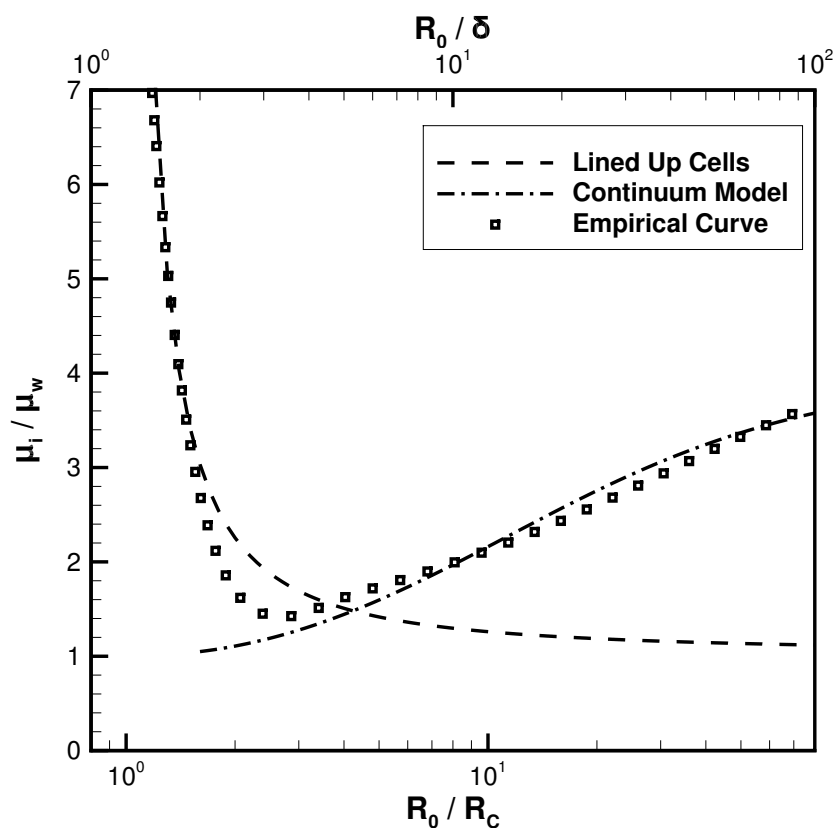
Figure 7: Prediction of the Fåhræus-Lindqvist effect by the two different models. The dashed line $---$ **represents the result for the lined up cells model while the** $-\cdot-\cdot-$ **curve is the result for the continuum model. These two results are compared with the empirical fit ($\square$) of the experimental results for in vitro blood flow by Pries et. al (Pries et al., 1994) for a hematocrit of** $55 \ \%$

In this case, for the continuum model, the result shown in the plot is the analytical one given by equation (46). The result for the lined up cells model is given numerically considering a parabolic profile for the cells.

The experimental data gives a minimum value of the intrinsic viscosity lower than the predicted by the theoretical model. The discrepancy is about 33 % greater than the experimental value. We argue that this difference can be related with the cell-cell hydrodynamic interaction and the irregularaties distribution in the microvessel wall, including the presence of other types of particles.

CILAMCE 2016

Proceedings of the *XXXVII Iberian Latin-American Congress on Computational Methods in Engineering*
Suzana Moreira Ávila (Editor), ABMEC, Braslia, DF, Brazil, November 6-9, 2016

Both asymptotic limits corresponding to the lined up cells and continuum model are in very good agreement with the experimental data. We can see that as $R_0/R_C \to 0$, the intrinsic viscosity rapidly increases when R_0 is about $2R_C$. In this limit the non-local characteristic of the blood viscosity has a very strong dependence on the geometry so that the blood can not be described by a continuum equivalent media. On the other hand, for large values of R_0/R_C the blood viscosity increases monotonically with R_0/R_C, tending to a saturation point for a suffcent large size of vessel $R_0 \sim 100R_C$. In this limit the intrinsic viscosity can be interpreted as an effective visocosity of the bulk blood.

5.2 Effects due to the presence of Yield Stress

When the red cells aggregate, it's necessary to make a minimum stress in order for the blood to flow. This minimum value for the stress is the yield stress τ_0. Using the continuum model for the blood flow it is possible to predict the effect of the yield stress on the intrinsic viscosity.

Figure 8 shows a plot of the blood intrinsic viscosity as a function of the non-dimensional yield stress for different values of the microvessel roughness. The increase of the intrinsic viscosity as the cells tends to aggregate can be seen. This effect is even stronger as the amplitude of the roughness increases. For instance, for a yield stress value of 0.4 we can see an increase in the intrinsic viscosity of 2% for α varying from 0 to 0.09. So the effect of the wall irregularities is very significant in a microcirculation regime.
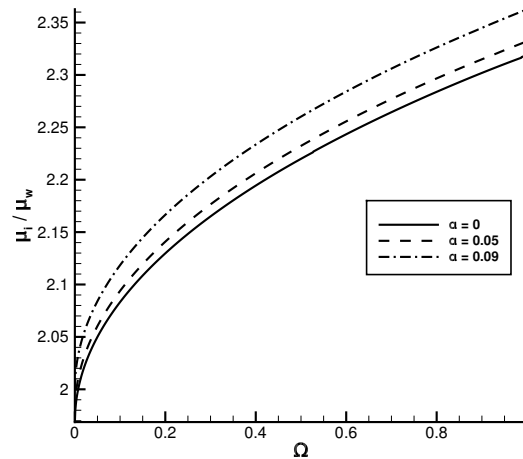
Figure 8: Intrinsic viscosity as a function of the nondimensional yield stress parameter Ω for $Re_w = 0.1$, $\chi = 0.9$, $\tilde{\mu}_p = 1$, $\tilde{\mu}_\infty = 4$ and different values of α.

It is important to discuss the range of this method. The condition for this method to work is that $R_B/R_\delta \le 1$. In that way we can define a critical value Ω_C, so that:

$$\Omega_C = \frac{\chi \tilde{G}_{min}}{Re_w} \qquad (71)$$

For a vessel of constant radius, where $\tilde{G} = \tilde{\mu}_i$ is a constant, we can trace a straight line to show the region where the numerical results represents the model. Out of this region, the model predicts that μ_i is a constant, as the whole core flow behaves like a rigid body.

6 Conclusion

In this work, we discussed the physical mechanisms in creeping flow which lead to the formation of the cell-depleted layer adjacent to the vessel wall. We also predicted the layer thickness in steady state, relating it to the main non-dimensional parameters which govern the mechanisms of the layer formation.

In addition, we studied the blood flow in two different scales (i.e. lower and upper bound limit) of the in vitro-microcirculation. Both the continuum model and our lined up cells model have shown good agreement with experimental data for the Fåhræus-Lindqvist. This models can be used to predict alterations in the blood viscosity due to blood abnormalities, which can be used to diagnose illnesses.

CILAMCE 2016

Proceedings of the *XXXVII Iberian Latin-American Congress on Computational Methods in Engineering*
Suzana Moreira Ávila (Editor), ABMEC, Braslia, DF, Brazil, November 6-9, 2016

Bibliography

Acrivos, A., Batchelor, G. K., Hinch, E. J., Koch, D. L. and Mauri, R. (1992). Longitudinal shear-induced diffusion of spheres in a dilute suspension, *Journal of fluid mechanics* **240**: 651–657.

Bird, R. B., Armstrong, R. C., Hassager, O. and Curtiss, C. F. (1977). *Dynamics of polymeric liquids*, Vol. 1, Wiley New York.

Chaffey, C., Brenner, H. and Mason, S. (1965). Particle motions in sheared suspensions, *Rheologica Acta* **4**(1): 64–72.

Chan, P.-H. and Leal, L. G. (1979). The motion of a deformable drop in a second-order fluid, *Journal of Fluid Mechanics* **92**(01): 131–170.

Cunha, F. R. and Hinch, E. J. (1996). Shear-induced dispersion in a dilute suspension of rough spheres, *Journal of Fluid Mechanics* **309**: 211–223.

Davis, R. H. (1996). Hydrodynamic diffusion of suspended particles: a symposium, *Journal of Fluid Mechanics* **310**: 325–335.

Einstein, A. (1956). *Investigations on the Theory of the Brownian Movement*, Courier Corporation.

Fåhræus, R. and Lindqvist, T. (1931). The viscosity of the blood in narrow capillary tubes, *American Journal of Physiology–Legacy Content* **96**(3): 562–568.

Kennedy, M. R., Pozrikidis, C. and Skalak, R. (1994). Motion and deformation of liquid drops, and the rheology of dilute emulsions in simple shear flow, *Computers & fluids* **23**(2): 251–278.

Kim, S. and Karrila, S. J. (2013). *Microhydrodynamics: principles and selected applications*, Courier Corporation.

Klingel, R., Fassbender, C., Fassbender, T., Erdtracht, B. and Berrouschot, J. (2000). Rheopheresis: rheologic, functional, and structural aspects, *Therapeutic Apheresis* **4**(5): 348–357.

Oliveira, T. F. and Cunha, F. R. (2011). A theoretical description of a dilute emulsion of very viscous drops undergoing unsteady simple shear, *Journal of Fluids Engineering* **133**(10): 101208.

Popel, A. S. and Johnson, P. C. (2005). Microcirculation and hemorheology, *Annual review of fluid mechanics* **37**: 43.

Pries, A., Secomb, T. W., Gessner, T., Sperandio, M. B., Gross, J. F. and Gaehtgens, P. (1994). Resistance to blood flow in microvessels in vivo., *Circulation research* **75**(5): 904–915.

Schowalter, W., Chaffey, C. and Brenner, H. (1968). Rheological behavior of a dilute emulsion, *Journal of colloid and interface science* **26**(2): 152–160.

Skalak, R., Ozkaya, N. and Skalak, T. C. (1989). Biofluid mechanics, *Annual review of fluid mechanics* **21**(1): 167–200.

Smart, J. R. and Leighton Jr, D. T. (1991). Measurement of the drift of a droplet due to the presence of a plane, *Physics of Fluids A: Fluid Dynamics (1989-1993)* **3**(1): 21–28.

Sung, K., Schmid-Schönbein, G., Skalak, R., Schuessler, G., Usami, S. and Chien, S. (1982). Influence of physicochemical factors on rheology of human neutrophils., *Biophysical journal* **39**(1): 101.